nanomaterials

MDPI

Article

Catalytic Preparation of Carbon Nanotubes from Waste Polyethylene Using FeNi Bimetallic Nanocatalyst

Kezhuo Li [1], Haijun Zhang [1,*], Yangfan Zheng [1], Gaoqian Yuan [1], Quanli Jia [2] and Shaowei Zhang [3,*]

1 The State Key Laboratory of Refractories and Metallurgy, Wuhan University of Science and Technology, Wuhan 430081, China; likezhuo0206@163.com (K.L.); 15671628617@163.com (Y.Z.); yuangaoqian@126.com (G.Y.)
2 Henan Key Laboratory of High Temperature Functional Ceramics, Zhengzhou University, 75 Daxue Road, Zhengzhou 450052, China; jiaquanli@zzu.edu.cn
3 College of Engineering, Mathematics and Physical Sciences, University of Exeter, Exeter EX4 4QF, UK
* Correspondence: zhanghaijun@wust.edu.cn (H.Z.); s.zhang@exeter.ac.uk (S.Z.); Tel.: +86-27-68862829 (H.Z); +44-7710166727 (S.Z.)

Received: 15 July 2020; Accepted: 28 July 2020; Published: 3 August 2020

Abstract: In this work, carbon nanotubes (CNTs) were synthesized by catalytic pyrolysis from waste polyethylene in Ar using an in-situ catalyst derived from ferric nitrate and nickel nitrate precursors. The influence factors (such as temperature, catalyst content and Fe/Ni molar ratio) on the formation of CNTs were investigated. The results showed that with the temperature increasing from 773 to 1073 K, the carbon yield gradually increased whereas the aspect (length-diameter) ratio of CNTs initially increased and then decreased. The optimal growth temperature of CNTs was 973 K. With increasing the Fe/Ni molar ratio in an FeNi bimetallic catalyst, the yield of CNTs gradually increased, whereas their aspect ratio first increased and then decreased. The optimal usage of the catalyst precursor (Fe/Ni molar ratio was 5:5) was 0.50 wt% with respect to the mass of polyethylene. In this case, the yield of CNTs reached as high as 20 wt%, and their diameter and length were respectively 20–30 nm, and a few tens of micrometers. The simple low-cost method developed in this work could be used to address the environmental concerns about plastic waste, and synthesize high value-added CNTs for a range of future applications.

Keywords: carbon nanotubes; waste polyethylene; ferric nitrate; nickel nitrate; catalytic pyrolysis

1. Introduction

As a lightweight, waterproof, and corrosion resistant material, plastic is widely used in almost every aspect of human society, contributing considerably to the economic growth and social sustainability [1]. However, the consistent increase in the accumulation of discarded plastics causes serious pollution to the environment due to their non-biodegradable nature under ambient conditions [2–4]. Currently, landfill and incineration are mainly used to dispose plastic waste, but they are becoming less and less acceptable due to their many demerits, e.g., waste of land and secondary pollution [5,6]. Hence, exploring a simple, low-cost and sustainable way to recycle plastic waste to form high value-added products, though very challenging, is of technical importance.

Carbon materials such as graphite, graphene and carbon nanotubes (CNTs) have attracted a lot of attention [7–16]. Among them, the last one, which possesses excellent properties such as low density, high tensile strength, high elastic modulus, and high thermal conductivity (>3000 $W \cdot m^{-1} \cdot K^{-1}$) [14–16], is used in the fields of composite materials [17], solar cells [18] and optical devices [19]. CNTs can be synthesized by arc discharge [20], flame synthesis [21], microwave-assisted synthesis [22], chemical

vapor deposition [23], and catalytic pyrolysis [24], among which, the last one has proved promising. With this method, polyolefin, which has a high carbon content, is usually used as the carbon source because the plastic waste is mostly hydrocarbon polymers [25–30]. This will not only enable the low cost production of novel CNTs but also address the above-mentioned issues caused by plastic waste accumulation and the conventional dumping methods.

In the plastic decomposition and carbon deposition process, the catalyst used plays a crucial role, which determines the morphology and structure of CNTs [31–33]. Conventional catalysts for the preparation of CNTs mainly include metallic iron, cobalt, nickel, and their compounds [34–36]. And bimetallic and polymetallic catalysts often perform better compared with monometallic counterparts. For example, by using $Ni(NO_3)_2{\cdot}0.6H_2O$, $Mg(NO_3)_2{\cdot}6H_2O$ and $(NH_3)_6Mo_7O_{24}{\cdot}0.4H_2O$ as catalyst precursors, and PEG200 as a solvent, Song et al. [25] firstly prepared Ni/Mo/MgO catalyst powders by a combustion method at 923 K, then prepared straight and double-helix multi-wall carbon nanotubes (MWNTs) respectively with diameters of about 30 and 60 nm from polypropylene powder under the role of the catalysts at 1123 K. Yang et al. [37] prepared Ni-Cu/MgO and Ni/MgO catalyst powders by sol-gel method from $Ni(NO_3)_2{\cdot}6H_2O$, $Mg(NO_3)_2{\cdot}6H_2O$ and $Cu(NO_3)_2{\cdot}3H_2O$ catalyst precursor, then used them to synthesize CNTs via thermal chemical vapor deposition method. They found that when Ni-Cu/MgO was used as a catalyst, the yield of CNTs was significantly higher than that used Ni/MgO, indicating that the incorporation of Cu enhanced the catalytic activity of Ni. By using a similar process, Baba et al. [38] firstly prepared CoO-MoO_3/MgO catalyst powder from $Co(CH_3COO)_2{\cdot}4H_2O$, $Mg(CH_3COO)_2{\cdot}4H_2O$ and $(NH_3)_6Mo_7O_{24}{\cdot}4H_2O$, then CNTs with "bamboo-like" structure were successfully formed from ethylene by using the catalyst at 923–1043 K. The combination of Mo with Co increased the carbon yield by about 20 times. Despite these positive results, there are still some problems with the catalytic pyrolysis processes, which need to be overcome, including, e.g., (1) the preparation process of bimetallic catalyst was complex, (2) relatively expensive catalysts were used and the overall production cost was high, and (3) the yield of CNTs was relatively low.

In addition, it is well known that CNTs prepared using Ni as catalyst have the advantages of high graphitization degree and good thermal stability, while Fe as catalyst has high catalytic activity and carbon solubility. Studies have also shown that the FeNi bimetallic catalysts had higher catalytic activity for catalytic pyrolysis of plastics due to the synergistic effect among components [39,40].

In the present work, CNTs were prepared from low cost waste polyethylene using inexpensive iron nitrate and nickel nitrate as catalyst precursors via simple catalytic pyrolysis method. The influence parameters of pyrolysis temperature, catalyst content and Fe/Ni molar ratio on the formation of CNTs were investigated.

2. Materials and Methods

2.1. Raw Materials

Powdery waste polyethylene (PE, ≥97.0%) was purchased from Shanghai Runwen Material Co. Ltd. (Shanghai, China). Commercial nickel nitrate ($Ni(NO_3)_2{\cdot}6H_2O$, analytically pure) and ferric nitrate ($Fe(NO_3)_3{\cdot}9H_2O$, analytically pure) supplied by Shanghai Sinopharm Chem. Co. Ltd. (Shanghai, China) were used as catalyst precursors. All the reagents were used directly. At the same time, it has been shown that the use of nitrate or chloride as catalyst precursors has no significant effect on the formation of CNTs in our previous work [6].

2.2. Sample Preparation

The process of CNTs preparation is as follows: Initially, nickel nitrate and ferric nitrate were dissolved respectively into 10 mL anhydrous ethanol. Next, they were combined in pairs in different molar ratios (the molar ratio of Fe/Ni was 10/0, 8/2, 6/4, 5/5, 4/6, 2/8 and 0/10, respectively) at room temperature (298 K) under vigorous agitation by a magnetic stirrer. The resultant solution was slowly dripped into the powdery waste polyethylene (the catalyst content was respectively 0.25, 0.50, 0.75 and 1.00 wt% of the weight of polyethylene) along the cup wall via equal volume method. Subsequently,

the waste polyethylene powder loaded with different catalysts precursors was obtained after 12 h drying at room temperature. Finally, the composite powder was subjected to 2 h heat treatment at 773, 873, 973, and 1073 K (the heating rate was 5 K/min) in an alumina-tube furnace, and the shielding gas was flowing argon (99.999 vol% purity).

2.3. Sample Characterization

The following equation was used to calculate the yield of carbon after the pyrolysis of waste polyethylene:

$$C = 1 - \frac{(m_2 - m_3) - m_4}{(m_1 - m_4)} \times 100\%$$

where, C is residual carbon rate, m_1 is the weight of composite powder, m_2 is the total weight of composite powder and alumina crucibles before pyrolysis, m_3 is the total weight of composite powder and alumina crucibles after pyrolysis, m_2–m_3 is the weight loss of waste polyethylene precursor before and after pyrolysis, and m_4 is the weight of adding Fe/Ni catalyst theoretically.

Phases in as-prepared samples were analyzed by X-ray powder diffraction (XRD) using a Philips X'Pert Pro diffractometer (PANalytical, Hillsboro, The Netherlands). The XRD spectra were recorded in the range from 10° to 90° (2θ) with a scanning rate of 2°/min, at 40 mA and 40 kV, using Cu$k\alpha$ radiation (λ = 0.1542 nm). Microstructure and phase morphologies of as-prepared samples were observed by means of a scanning electron microscope (SEM; Nova400NanoSEM, 15 kV, Amsterdam, Netherlands), a transmission electron microscope (TEM; JEM-2100UHRSTEM, 200 kV, Tokyo, Japan) with an energy dispersive spectrometer (EDS, Penta FET X-3 Si (Li)), and a high-resolution TEM (HRTEM; JEM-3010, 300 kV). N_2 adsorption-desorption isotherms were examined on an automatic surface area and pore size analyzer (Autosorb-1, Quantachrome Instruments, Boynton Beach, FL, USA). The surface area was calculated from the adsorption branch of the isotherms using non-local density functional theory, and pore size distribution was calculated using Barrett–Joyner–Halanda model.

3. Results and Discussion

3.1. Effects of Pyrolysis Temperature on the Growth of CNTs

Figure 1 shows XRD patterns of samples obtained at 773–1073 K using 0.50 wt% $Fe_{50}Ni_{50}$ (the molar ratio of Fe/Ni was 5/5) bimetallic catalysts. At 773 K, a broad diffraction peak appeared at around 26° (2θ), indicating the formation of graphitic carbon in the sample. Furthermore, at 44.2 and 51.5°, two weak diffraction peaks were observed, respectively belonging to the (111) and (200) planes of $FeNi_3$ (ICDD card: No. 03-065-3244). As the pyrolysis temperature increased to 873 K, the peak height of graphitic carbon increased evidently. With further increasing the pyrolysis temperature to 973 K, the diffraction peak (about 26°) of graphitic carbon became the sharpest, and well matched to the characteristic (002) plane of graphite (ICDD card: No. 01-075-1621), revealing the highest graphitization degree of the carbon. However, the pyrolysis temperature further increasing to 1073 K led to the peak height of the carbon decreased slightly. The above results suggested that under the test conditions, 973 K was the optimal temperature for CNTs formation.

Presented in Figure 2 are SEM images of samples whose XRD patterns are displayed in Figure 1, demonstrating significant effects of the temperature on the phase morphology. At 773 K, a relatively small number of short CNTs were generated (Figure 2a). When the pyrolysis temperature increased to 873 K, the yield and lengths of CNTs increased (Figure 2b). Upon the pyrolysis temperature further increasing to 973 K, many more CNTs with relatively small diameters of about 20 nm and lengths of a few tens of micrometers were formed (Figure 2c). However, while the pyrolysis temperature further increased to 1073 K, thicker and shorter CNTs were obtained, which might be due to the relatively high temperatures that cause the catalyst particles to aggregate (Figure 2d). The SEM observations in Figure 2 conclude that the optimal formation temperature of CNTs was at 973 K, which was in agreement with that suggested by the XRD presented in Figure 1.

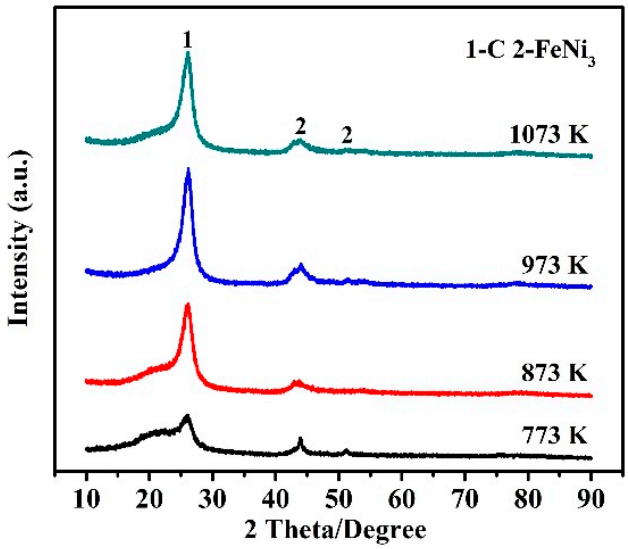

Figure 1. XRD patterns of samples prepared at different pyrolysis temperatures, with 0.50 wt% $Fe_{50}Ni_{50}$ bimetallic catalysts.

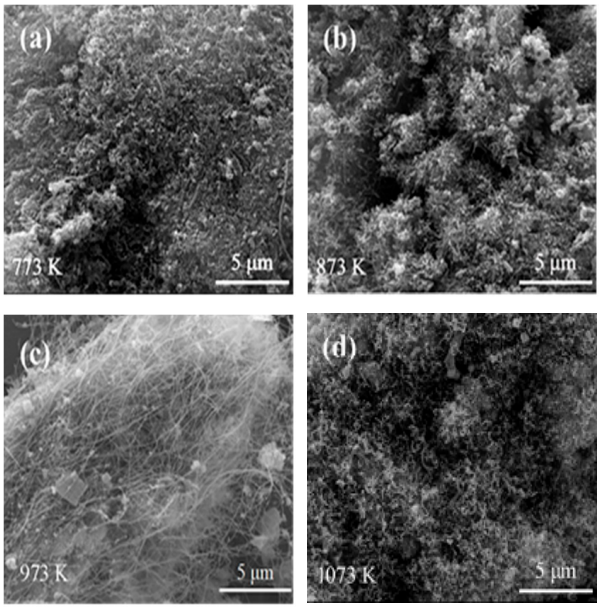

Figure 2. SEM images of samples obtained with 0.50 wt% $Fe_{50}Ni_{50}$ bimetallic catalysts at: (**a**) 773 K, (**b**) 873 K, (**c**) 973 K, and (**d**) 1073 K.

3.2. *Effects of Catalyst Amount on the Growth of CNTs*

XRD patterns of the samples fired at 973 K corresponding to different amounts of $Fe_{50}Ni_{50}$ bimetallic catalysts are shown in Figure 3, indicating that the amount of catalysts had only a minor effect on the phase formation in the product. When 0.25 wt% $Fe_{50}Ni_{50}$ bimetallic catalysts was added, a broad carbon diffraction peak appeared at around 26° (2θ) and two weak diffraction peaks of $FeNi_3$ were also seen. With increasing the catalyst content to 0.50 wt%, the carbon diffraction peak became sharper and narrower. With further increasing the catalyst content to 0.75 wt%, the carbon diffraction peak almost did not change. When the catalyst content was finally increased to 1.00 wt%, the carbon diffraction peak decreased significantly. Thus, it can be reasonably concluded that the optimal catalyst amount required for CNTs formation was 0.50–0.75 wt%.

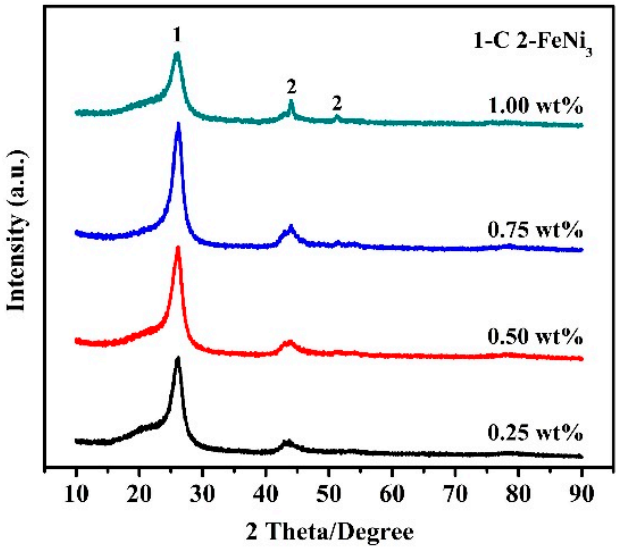

Figure 3. XRD patterns of samples obtained with various amounts of $Fe_{50}Ni_{50}$ bimetallic catalysts at 973 K.

Figure 4 gives SEM images of the samples whose XRD patterns are presented in Figure 3, revealing the generation of CNTs with fine diameters in the samples, and the content of $Fe_{50}Ni_{50}$ bimetallic catalysts has a great influence on CNTs yield. As evidenced by Figure 4a, an extremely few number of CNTs were detected in the sample using 0.25 wt% $Fe_{50}Ni_{50}$ bimetallic catalysts. However, as the content of the catalyst increased to 0.50 wt%, many more CNTs with smaller diameters and lengths up to a few tens of micrometers were generated (Figure 4b). With the content of $Fe_{50}Ni_{50}$ bimetallic catalysts further increasing to 0.75 wt%, the CNTs were bent and intertwined despite increase in yield (Figure 4c). When the catalyst content was finally increased to 1.00 wt%, short and thick CNTs were formed and entangled together (Figure 4d). These results demonstrated that the addition of 0.50 wt% $Fe_{50}Ni_{50}$ bimetallic catalysts was best suitable for the growth of CNTs.

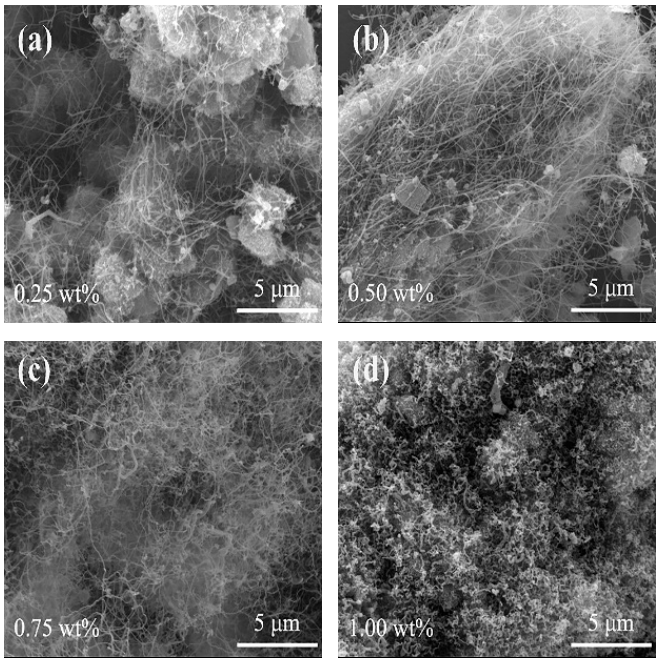

Figure 4. SEM images of samples obtained at 973 K with various amounts of $Fe_{50}Ni_{50}$ bimetallic catalysts: (**a**) 0.25 wt%, (**b**) 0.50 wt%, (**c**) 0.75 wt% and (**d**) 1.00 wt%.

3.3. Effects of Fe/Ni molar Ratio on the Growth of CNTs

Figure 5 presents XRD patterns of samples fired at 973 K versus the molar ratio of Fe/Ni in FeNi catalyst (0.50 wt% was used), revealing the effect of the latter on the phase composition. When iron only was added as the catalyst, graphite carbon, iron and iron carbide were present as the primary phases, and when nickel only was used as the catalyst, poorly crystalline graphitic carbon (indicated by the broad peak at 26° (2θ)), along with Ni was detected. On the other hand, when the FeNi catalyst was used, graphitic carbon (ICDD card: No. 01-075-1621) became the dominant crystalline phase, along with $FeNi_3$ (ICDD card: No. 03-065-3244) and Fe_2O_3 (ICDD card: No. 00-001-1053). In addition, with the Fe/Ni molar ratio in the catalyst increasing from 2/8 to 8/2, the graphitic carbon initially increased but then decreased. Moreover, the highest graphitic carbon peak was seen in the case of using the catalyst with the Fe/Ni molar ratio of 5/5, implying the highest graphitization degree of the carbon. These results suggested that the Fe/Ni molar ratio of 5/5 was best suitable for the formation of CNTs.

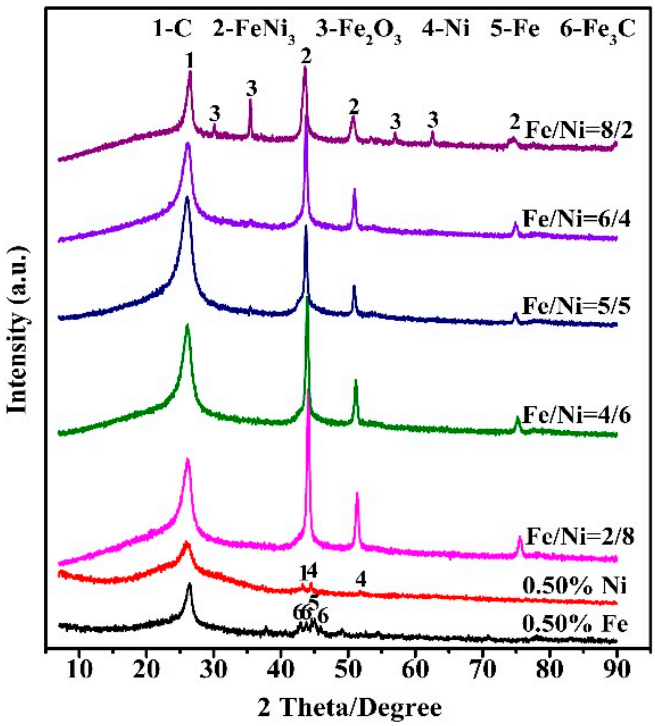

Figure 5. XRD patterns of product samples obtained at 973 K for 2 h, using 0.50 wt% Fe or Ni single metal catalyst and FeNi bimetallic catalyst (Fe/Ni molar ratio between 2/8 and 8/2, in total 0.50 wt%).

Figure 6 shows SEM images of the samples whose XRD patterns are presented in Figure 5, demonstrating the significant influence of the Fe/Ni molar ratio on the CNTs morphology. A few short and thick CNTs were generated when using 0.50 wt% iron catalyst (Figure 6a), whereas much curved CNTs were formed and entangled together when using 0.50 wt% nickel catalyst (Figure 6b). With Fe/Ni molar ratio increasing from 2/8 to 4/6, there was no obvious formation of CNTs in the sample (Figure 6c,d). However, upon increasing the molar ratio of Fe/Ni to 5/5, a large number of CNTs with diameters of 20–30 nm and lengths of a few tens of micrometers were formed (Figure 6e). Upon further increasing the Fe/Ni molar ratio to 6/4, thinner and longer CNTs were produced and entangled together (Figure 6f). Finally, when the Fe/Ni molar ratio reached 8/2, fewer CNTs with lengths of a few micrometers and diameters of 30–40 nm were formed (Figure 6g). According to the above results, the optimal Fe/Ni molar ratio for preparation of CNTs should be 5/5, which was in agreement with that suggested by the XRD results in Figure 5.

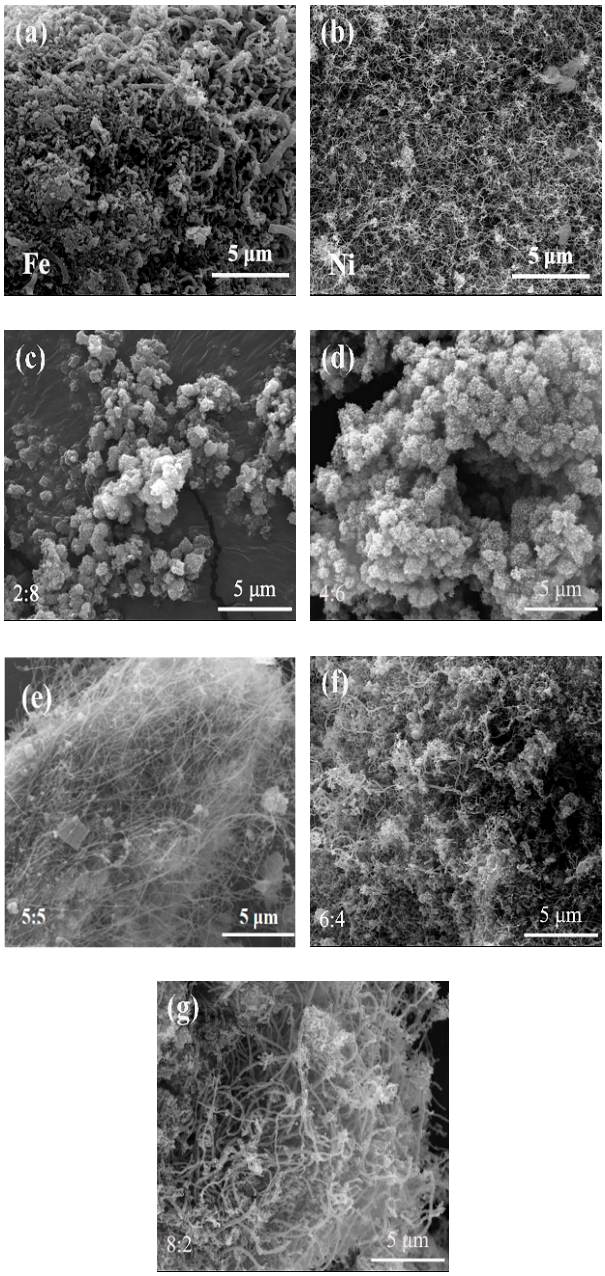

Figure 6. SEM images of product samples obtained at 973 K for 2 h using 0.50 wt% FeNi catalysts with different Fe/Ni molar ratio: (**a**) Fe, (**b**) Ni, (**c**) Fe/Ni = 2/8, (**d**) Fe/Ni = 4/6, (**e**) Fe/Ni = 5/5, (**f**) Fe/Ni = 6/4, and (**g**) Fe/Ni = 8/2.

Presented in Figure 7 are the effects of Fe/Ni molar ratio in the FeNi catalyst (in total 0.50 wt%) on the carbon yield in the product samples obtained at 973 K for 2 h, verifying that the carbon yield under the circumstance of using a bimetallic catalyst was much higher than that under the circumstance of using a single metal catalyst. The carbon yield was only about 7 % and 8 % when using 0.50 wt% single metal iron and nickel. However, when the same amount of FeNi bimetallic catalyst was used, the carbon yield increased significantly. Moreover, with the Fe/Ni molar ratio in the catalyst increasing from 2/8 to 8/2, the carbon yield increased from 18 % to 22 %. In addition, the diameter, length and carbon yield of as-prepared CNTs using FeNi bimetallic catalysts and corresponding monometallic counterpart were compared (as shown in Table 1). It shows that the quality (diameter and length) of CNTs prepared by present FeNi bimetallic catalysts in this work was better. Although the carbon yield of samples prepared in some literatures [39,40] was higher, however, it should be emphasized that the

length of the CNTs was shorter and the amount of the catalyst was much higher. At the same time, the yield and quality of CNTs prepared by FeNi bimetallic catalysts in this work were superior to the corresponding monometallic one. These results indicated that the FeNi bimetallic catalysts performed much better than the single Fe or Ni catalysts in enhancing the carbon yield, and catalyzing the growth of CNTs.

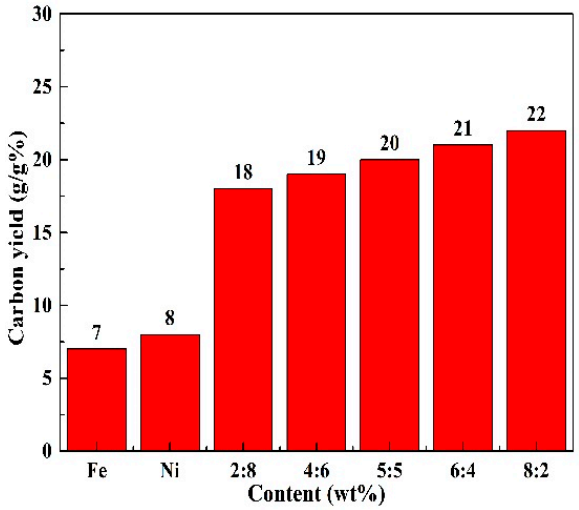

Figure 7. Carbon yield of product samples prepared at 973 K for 2 h, as a function of Fe/Ni molar ratio in the FeNi catalyst (in total: 0.50 wt%).

Table 1. Comparison of diameter, length and carbon yield of as-prepared CNTs using FeNi bimetallic and corresponding single metal as a catalyst.

Raw Material	Catalyst Type	Catalyst Addition (wt%)	Temperature (K)	CNTs Diameter (nm)	CNTs Length (μm)	Carbon Yield (wt%)	Reference
PE	FeNi	0.50	973	20–30	few tens	20	This work
PE	Fe	0.50	973	thick	shorter	7	This work
PE	Ni	0.50	973	thick	curved	8	This work
PE	Ni	0.75	973	30–50	tens	17	[6]
Mixing plastic	FeNi	5.00	1023	10–40	shorter	46	[39]
PP	FeNi	5.00	1023	20–50	shorter	41	[40]

PE: polyethylene; PP: polypropylene.

3.4. TEM/HRTEM Characterization of CNTs

TEM, HRTEM and EDS were used to characterize the morphology and microstructure of CNTs prepared under optimal conditions (973 K/2 h and 0.50 wt% $Fe_{50}Ni_{50}$ bimetallic catalysts). As displayed in Figure 8a, CNTs exhibited a clear hollow structure, with a length of a few tens of micrometers and diameter of 20–30 nm. HRTEM further reveals that the interlayer spacing of CNTs was 0.34 nm, which was consistent with the standard graphitic interlayer spacing of the (002) plane (0.34 nm), demonstrating the high crystallinity of the CNTs (Figure 8b). Some nanoparticles of about 10 nm in size were found at the tips and inside of some CNTs (indicated by the white circles in Figure 8a); they were verified by EDS (Figure 8c) to be FeNi nanoparticles. The above results indicate that FeNi bimetallic nanoparticles were prepared under the experimental conditions and acted as a catalyst to catalyze the pyrolysis of waste polyethylene to produce CNTs. Meanwhile, Figure 8a as well as our previous work [6] proved that catalyst particles always existed inside or at the tip of CNTs.

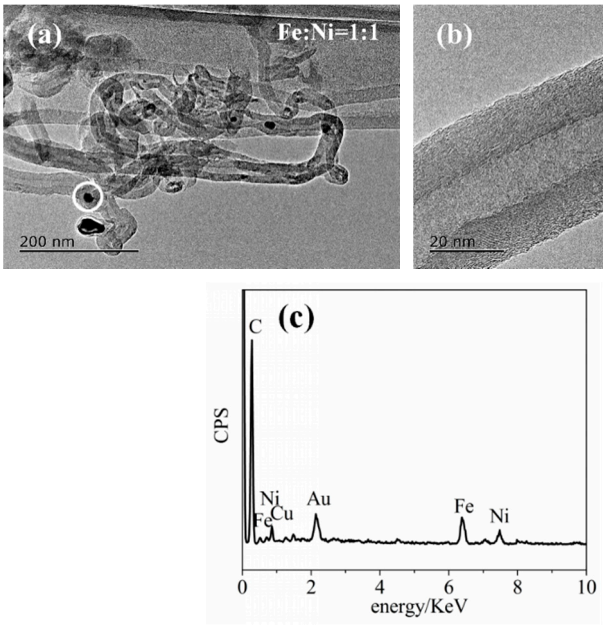

Figure 8. TEM and HRTEM images of product samples obtained at 973 K for 2 h using 0.50 wt% $Fe_{50}Ni_{50}$ nanocatalyst: (**a**) TEM image of CNTs, (**b**) HRTEM image of an individual CNT, and (**c**) EDS of the nanoparticles circled in Figure 8a.

Nitrogen adsorption-desorption measurements were carried out to determine the specific surface area and pore size distribution of CNTs prepared under the optimal experimental conditions (973 K/2 h and 0.50 wt% $Fe_{50}Ni_{50}$ bimetallic catalysts), as shown in Figure 9. The CNTs presented a typical type III isotherm when the relative pressure (P/P_0) was between 0.1 and 1.0 (Figure 9a), and based on the BET model, the specific surface areas of CNTs prepared under the optimal experimental conditions was calculated as 139.2 $m^2 \cdot g^{-1}$. Furthermore, the pore size distribution was calculated using Barrett–Joyner–Halanda model (Figure 9b), it was proved that the average pore size of the CNTs prepared was about 11.7 nm.

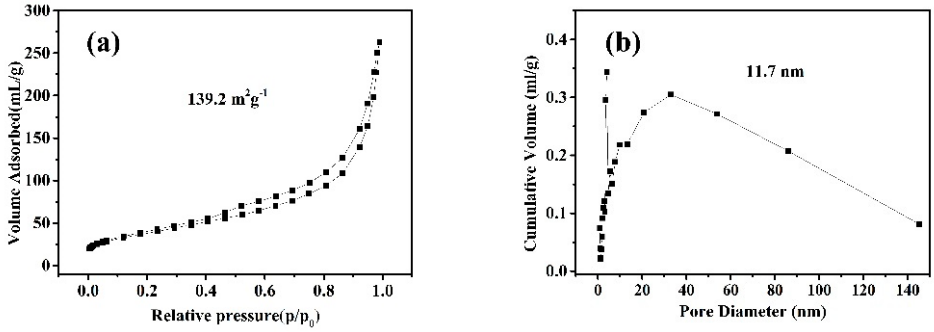

Figure 9. N_2 adsorption-desorption isotherms of CNTs prepared under the optimal experimental conditions. Nitrogen adsorption/desorption isotherms (**a**) and BJH pore size distribution profiles (**b**) of as-prepared CNTs. (2 h catalytic pyrolysis at 973 K with 0.50 wt% $Fe_{50}Ni_{50}$ bimetallic catalysts).

4. Conclusions

CNTs with a diameter of 20–30 nm and length of a few tens of micrometers were synthesized by simple catalytic pyrolysis of inexpensive polyethylene in Ar using cheap ferric nitrate and nickel nitrate as catalyst precursors. XRD, EDS and TEM confirmed that FeNi bimetallic nanoparticles were formed in-situ from the ferric nitrate and nickel nitrate catalyst precursors during the pyrolysis process, and they acted as the catalysts to produce CNTs from waste polyethylene. Compared to their single metal counterparts, the FeNi bimetallic catalysts performed much better. The optimal condition for the generation of CNTs in this work was: using 0.50 wt% $Fe_{50}Ni_{50}$ bimetallic catalysts, catalytic pyrolysis

2 h at 973 K. The work reported here could be potentially used to address the current concerns about plastic waste and to convert a range of plastic waste to high value-added CNTs.

Author Contributions: K.L. did experimental work and wrote the paper; H.Z., S.Z. and Q.J. designed and reviewed the manuscript and provided some suggestions; Y.Z. did experimental work; G.Y. reviewed the manuscript and assisted in the experimental work. All authors contributed to and critically reviewed the manuscript. H.Z. and S.Z. made particularly major contributions to the writing and editing. All authors have read and agreed to the published version of the manuscript.

Funding: This work was financially supported by National Natural Science Foundation of China (Grant No. 51872210 and 51672194), Program for Innovative Teams of Outstanding Young and Middle-aged Researchers in the Higher Education Institutions of Hubei Province (T201602), and Key Program of Natural Science Foundation of Hubei Province, China (Grant/Award Number: 2017CFA004).

Conflicts of Interest: The authors declare no conflict of interest.

References

1. Sharuddin, S.D.A.; Abnisa, F.; Daud, W.M.A.W.; Aroua, M.K. A review on pyrolysis of plastic wastes. *Energy Convers. Manag.* **2016**, *115*, 308–326. [CrossRef]
2. Acomb, J.C.; Wu, C.; Williams, P.T. The use of different metal catalysts for the simultaneous production of carbon nanotubes and hydrogen from pyrolysis of plastic feedstocks. *Appl. Catal. B* **2016**, *180*, 497–510. [CrossRef]
3. Li, G.; Tan, S.; Song, R.; Tang, T. Synergetic effects of molybdenum and magnesium in Ni-Mo-Mg catalysts on the one-step carbonization of polystyrene into carbon nanotubes. *Ind. Eng. Chem. Res.* **2017**, *56*, 11734–11744. [CrossRef]
4. Bajad, G.; Guguloth, V.; Vijayakumar, R.P.; Bose, S. Conversion of plastic waste into CNTs using Ni/Mo/MgO catalyst-an optimization approach by mixture experiment. *Fullerenes Nanotubes Carbon Nanostruct.* **2016**, *24*, 162–169. [CrossRef]
5. Zhuo, C.; Levendis, Y.A. Upcycling waste plastics into carbon nanomaterials: A review. *J. Appl. Polym. Sci.* **2013**, *131*, 39931–39945. [CrossRef]
6. Zheng, Y.; Zhang, H.; Ge, S.; Song, J.; Wang, J.; Zhang, S. Synthesis of carbon nanotube arrays with high aspect ratio *via* Ni-catalyzed pyrolysis of waste polyethylene. *Nanomaterials* **2018**, *8*, 556. [CrossRef]
7. Ding, D.H.; Chong, X.H.; Xiao, G.Q. Combustion synthesis of B4C/Al_2O_3/C composite powders and their effects on properties of low carbon MgO-C refractories. *Ceram. Int.* **2019**, *45*, 16433–16441. [CrossRef]
8. Tian, C.; Yu, J.; Yuan, L.; Jin, E.; Wen, T.; Jia, D.; Liu, Z. Effect of interfacial reaction behaviour on the clogging of SEN in the continuous casting of bearing steel containing rare earth elements. *J. Alloys Compd.* **2019**, *792*, 1–7. [CrossRef]
9. Chen, Y.; Deng, C.; Wang, X.; Ding, J.; Yu, C.; Zhu, H. Effect of Si powder-supported catalyst on the microstructure and properties of Si_3N_4-MgO-C refractories. *Constr. Build. Mater.* **2020**, *240*, 117964. [CrossRef]
10. Wang, Q.; Li, Y.; Jin, S. Enhanced mechanical properties of Al_2O_3-C refractories with silicon hybridized expanded graphite. *Mater. Sci. Eng. A* **2018**, *709*, 160–171. [CrossRef]
11. Gu, Q.; Ma, T.; Zhao, F.; Jia, Q.L.; Liu, X. Enhancement of the thermal shock resistance of MgO-C slide plate materials with the addition of Nano-ZrO_2 modified magnesia aggregates. *J. Alloys Compd.* **2020**. [CrossRef]
12. Ding, D.; Lv, H.; Xiao, Q. Improved properties of low-carbon MgO-C refractories with the addition of multilayer graphene/$MgAl_2O_4$ composite powders. *Int. J. Appl. Ceram. Technol.* **2020**, *17*, 645–656. [CrossRef]
13. Liu, M.; Huang, T.; Xiong, M. Micro-Nano Carbon Structures with Platelet, Glassy and Tube-Like Morphologies. *Nanomaterials* **2019**, *9*, 1242. [CrossRef] [PubMed]
14. Dresselhaus, M.S.; Dresselhaus, G.; Charlier, J.C.; Hernández, E. Electronic, thermal and mechanical properties of carbon nanotubes. *Philos. Trans. R. Soc. Lond. Ser. A Math. Phys. Eng. Sci.* **2004**, *362*, 2065–2098. [CrossRef]
15. Terrones, M. Carbon nanotubes: Synthesis and properties, electronic devices and other emerging applications. *Int. Mater. Rev.* **2013**, *49*, 325–377. [CrossRef]
16. Zhang, Z.; Dewan, C.; Kothari, S.; Mitra, S.; Teeters, D. Carbon nanotube synthesis, characteristics, and microbattery applications. *Mater. Sci. Eng. B* **2005**, *116*, 363–368. [CrossRef]
17. Kausar, A.; Rafique, I.; Muhammad, B. Review of applications of polymer/carbon nanotubes and epoxy/CNT composites. *Polym.-Plast. Technol. Eng.* **2016**, *55*, 1167–1191. [CrossRef]

18. Jeon, I.; Matsuo, Y.; Maruyama, S. Single-walled carbon nanotubes in solar cells. *Top. Curr. Chem. (Cham)* **2018**, *376*, 4–32. [CrossRef]
19. Tan, Y. Chemical sensing applications of carbon nanotube-deposited optical fibre sensors. *Chemosensors* **2018**, *6*, 55. [CrossRef]
20. Zhao, T.K.; Ji, X.L.; Jin, W.B.; Yang, W.B.; Li, T.H. Coral-like amorphous carbon nanotubes synthesized by a modified arc discharge. *Fullerenes Nanotubes Carbon Nanostruct.* **2017**, *25*, 359–362. [CrossRef]
21. Sun, B.; Cao, W.; Guo, Y.; Wang, Y.; Luo, J.; Jiang, P. Flame pyrolysis synthesis of self-oriented carbon nanotubes. *AIP Adv.* **2013**, *3*, 56–61.
22. Kure, N.; Hamidon, M.N.; Azhari, S.; Mamat, N.S.; Yusoff, H.M.; Isa, B.M.; Yunusa, Z. Simple microwave-assisted synthesis of carbon nanotubes using polyethylene as carbon precursor. *J. Nanomater.* **2017**, *2017*, 2474267. [CrossRef]
23. Li, Y.; Zhang, X.; Tao, X.; Xu, J.; Chen, F.; Shen, L.; Yang, X.; Liu, F.; Tendeloo, G.V.; Geise, H.J. Single phase $MgMoO_4$ as catalyst for the synthesis of bundled multi-wall carbon nanotubes by CVD. *Carbon* **2005**, *43*, 1325–1328. [CrossRef]
24. Song, J.; Zhang, H.; Wang, J.; Huang, L.; Zhang, S. High-yield production of large aspect ratio carbon nanotubes *via* catalytic pyrolysis of cheap coal tar pitch. *Carbon* **2018**, *130*, 701–713. [CrossRef]
25. Song, R.; Ji, Q. Synthesis of carbon nanotubes from polypropylene in the presence of Ni/Mo/MgO Catalysts *via* combustion. *Chem. Lett.* **2011**, *40*, 1110–1112. [CrossRef]
26. Kadapure, S.A.; Arush, K.; Sagar, C.; Shreshtha, S.; Sangeeta, M.; Sukanya, J.; Devdatt, R.T.; Sabhya, S.; Navya, B.L.; Amit, T. Tertiary recycling of waste plastic using catalytic cracking into crude oil. *Energy Sources Part A* **2016**, *38*, 2942–2948. [CrossRef]
27. Miskolczi, N.; Sója, J.; Tulok, E. Thermo-catalytic two-step pyrolysis of real waste plastics from end of life vehicle. *J. Anal. Appl. Pyrolysis.* **2017**, *128*, 1–12. [CrossRef]
28. Almeida, D.; Marques, M. Thermal and catalytic pyrolysis of plastic waste. *Polímeros* **2016**, *26*, 44–51. [CrossRef]
29. Wu, C.; Wang, Z.; Wang, L.; Williams, P.T.; Huang, J. Sustainable processing of waste plastics to produce high yield hydrogen-rich synthesis gas and high quality carbon nanotubes. *R. Soc. Chem. Adv.* **2012**, *2*, 4045–4047. [CrossRef]
30. He, M.; Xiao, B.; Hu, Z.; Liu, S.; Guo, X.; Luo, S. Syngas production from catalytic gasification of waste polyethylene: Influence of temperature on gas yield and composition. *Int. J. Hydrog. Energy* **2009**, *34*, 1342–1348. [CrossRef]
31. Zhou, L.-P.; Ohta, K.; Kuroda, K.; Lei, N.; Matsuishi, K.; Gao, L.; Matsumoto, T.; Nakamura, J. Catalytic functions of Mo/Ni/MgO in the synthesis of thin carbon nanotubes. *J. Phys. Chem. B* **2004**, *109*, 4439–4447. [CrossRef]
32. Liu, W.-W.; Aziz, A.; Chai, S.-P.; Mohamed, A.R.; Hashim, U. Synthesis of single-walled carbon nanotubes: Effects of active metals, catalyst supports, and metal loading percentage. *J. Nanomater.* **2013**, 110–114. [CrossRef]
33. Shen, Y.; Gong, W.; Zheng, B.; Gao, L. Ni-Al bimetallic catalysts for preparation of multiwalled carbon nanotubes from polypropylene: Influence of the ratio of Ni/Al. *Appl. Catal. B* **2016**, *181*, 769–778. [CrossRef]
34. Tan, S.-M.; Chai, S.-P.; Liu, W.-W.; Mohamed, A.R. Effects of FeO_x, CoO_x, and NiO catalysts and calcination temperatures on the synthesis of single-walled carbon nanotubes through chemical vapor deposition of methane. *J. Alloys Compd.* **2009**, *477*, 785–788. [CrossRef]
35. Ago, H.; Uehara, N.; Yoshihara, N.; Tsuji, M.; Yumura, M.; Tomonaga, N.; Setogucjo, T. Gas analysis of the CVD process for high yield growth of carbon nanotubes over metal-supported catalysts. *Carbon* **2006**, *44*, 2912–2918. [CrossRef]
36. Chai, S.-P.; Sharif., S.H.; Mohamed, A.R. The effect of catalyst calcination temperature on the diameter of carbon nanotubes synthesized by the decomposition of methane. *Carbon* **2007**, *45*, 1535–1541. [CrossRef]
37. Yang, W.; Feng, Y.; Chu, W. Catalytic chemical vapor deposition of methane to carbon nanotubes: Copper promoted effect of Ni/MgO catalysts. *J. Nanotechnol.* **2014**, *2014*, 547030. [CrossRef]
38. Baba, M.S.; Sano, H.; Zheng, G.-B.; Uchiyama, Y. Effect of Mo in Co-Mo/Mgo catalysts on the synthesis yield and structure of carbon nanotubes. *J. Ceram. Soc. Jpn.* **2009**, *117*, 654–658. [CrossRef]

39. Yao, D.; Wu, C.; Yang, H.; Zhang, Y.; Nahil, M.; Chen, Y.; Williams, P.T.; Chen, H. Co-production of hydrogen and carbon nanotubes from catalytic pyrolysis of waste plastics on Ni-Fe bimetallic catalyst. *Energy Convers. Manag.* **2017**, *148*, 692–700. [CrossRef]
40. Cai, N.; Yang, H.P.; Zhang, X.; Xia, S.W.; Yao, D.D.; Bartocci, P.; Fantozzi, F.; Chen, Y.Q.; Chen, H.P.; Williams, P.T. Bimetallic carbon nanotube encapsulated Fe-Ni catalysts from fast pyrolysis of waste plastics and their oxygen reduction properties. *Waste Manag.* **2020**, *109*, 119–126. [CrossRef]